COMMUNICATION

Designed Synthesis of Coaxial SnO_2@carbon Hollow Nanospheres for Highly Reversible Lithium Storage

By *Xiong Wen Lou,* Chang Ming Li,* and *Lynden A. Archer**

Lithium-ion batteries (LIBs) are unmatched among energy storage technologies in terms of power density per unit volume or per unit mass.[1–6] SnO_2-based nanostructured materials are attracting growing research attention as high-capacity negative electrodes for LIBs for a variety of reasons, including their high theoretical capacity, low cost, low toxicity, and widespread availability.[2] In a SnO_2-based LIB electrode, two principal electrochemical processes occur: $SnO_2 + 4Li^+ + 4e^- \rightarrow Sn + 2Li_2O$ (1); $Sn + xLi^+ + xe^- \leftrightarrow Li_xSn$ ($0 \leq x \leq 4.4$) (2). The first reaction is irreversible, and leads to an initial fall-off in the capacity of the electrode during the first few charge–discharge cycles. The second process is reversible, and by cycling between the alloyed, Li_xSn, and de-alloyed, Sn, states, lithium can be repeatedly released and stored. The theoretical reversible lithium storage capacity for the second reaction is readily calculated to be 790 mA h g^{-1}, which is more than twice the theoretical capacity, 372 mA h g^{-1}, for currently used graphite.[2,3,7–9]

Despite their superior theoretical storage capacity, SnO_2-based anodes have underperformed as LIB anodes. This is traced to their poor capacity retention over extended charge–discharge cycling.[1] The extremely large volume change produced by the alloying reaction with Li (the volume change is about 250% when Sn alloys with Li to form $Li_{4.4}Sn$)[10] is widely believed to be the source of this behavior. Specifically, these large cyclic volume changes are believed to create commensurately large cyclic stresses in the SnO_2 anode materials, leading fatigue failure and disintegration of the active material. This so-called pulverization problem causes a breakdown in electrical contact pathways between adjacent particles, leading to rapid capacity fading.[1]

Because the source of pulverization is of fundamental electrochemical origin, its mitigation has proven quite difficult. One strategy is to design the nanostructure of electrode materials.[3,5,11] For example, if the SnO_2 anode comprises hollow and/or porous nanostructures, the local empty space in the structures can partially accommodate the large volume change, delaying capacity fading.[12–20] Another commonly used approach is to use nanocomposite materials (e.g., the inactive/active concept).[1] In particular, nanopainting with carbon has recently been found effective for improving cyclability, where carbon functions as a physical buffering layer for the large volume change (cushion effect).[7,9,14,21–23] For example, the recent commercial SONY tin-based anode has been characterized by Whittingham and coworkers to be basically composed of amorphous SnCo nanoparticles coated with graphitic carbon.[24] Despite the physical appeal of these procedures, our recent studies show that either design strategy alone leads to only limited improvement in cyclability of SnO_2-based anode materials.[13,25,26]

Herein, we propose a new type of nanoarchitecture, coaxial SnO_2@carbon hollow nanospheres, which integrates both aforementioned design principles. We show that anodes comprised of this structure manifest exceptional cycling performance and charge-rate capabilities. The schematic shown in Figure 1 illustrates our concept. In step 1, silica nanospheres (about 240–250 nm in diameter) are coated with uniform SnO_2 double-shells employing a recently developed protocol.[27] The double-shelled architecture is advantageous because it increases not only the structural integrity of the active material, but also enhances the weight fraction of the electrochemically active component (SnO_2) in the designed composite anode. In step 2, these core/shell silica@SnO_2 nanospheres are coated with glucose-derived carbon-rich polysaccharide (GCP) by a simple hydrothermal approach. It is well known that such GCP contains abundant hydroxyl groups, and can be carbonized at a relatively low temperature in an inert atmosphere.[28] After carbonization, the silica nanotemplates are removed in the final step 3, to produce SnO_2@carbon coaxial hollow nanospheres.

We first examined the morphology and microstructure of the as-derived SnO_2@carbon hollow nanospheres with field-emission scanning electron microscopy (FESEM) and transmission electron microscopy (TEM). From the FESEM images (Fig. 2a, b), it can be clearly observed that the shells of a significant fraction of hollow spheres are collapsed upon template removal, like deflated balloons, but not broken. This effect is likely caused by the contraction stress exerted from the carbon shell due to significant shrinkage of GCP during carbonization. As a result, the carbon shell is tightly attached to the SnO_2 shell (Fig. 2c, d), which is beneficial for mechanical reinforcement and for enhancing electronic conduction. By comparison, bare SnO_2

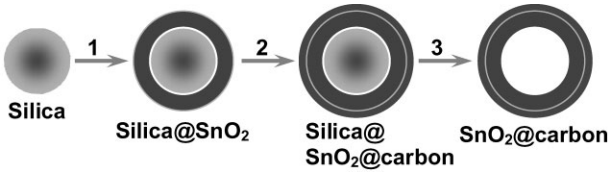

Figure 1. Schematics of formation of SnO_2@carbon coaxial hollow spheres.

[*] Dr. X. W. Lou, Prof. L. A. Archer
School of Chemical and Biomolecular Engineering
Cornell University, Ithaca, NY 14853-5201 (USA)
E-mail: laa25@cornell.edu; xwlou@ntu.edu.sg
Dr. X. W. Lou, Prof. C. M. Li
School of Chemical and Biomedical Engineering
Nanyang Technological University
70 Nanyang Drive, Singapore 637457 (Singapore)

DOI: 10.1002/adma.200803439

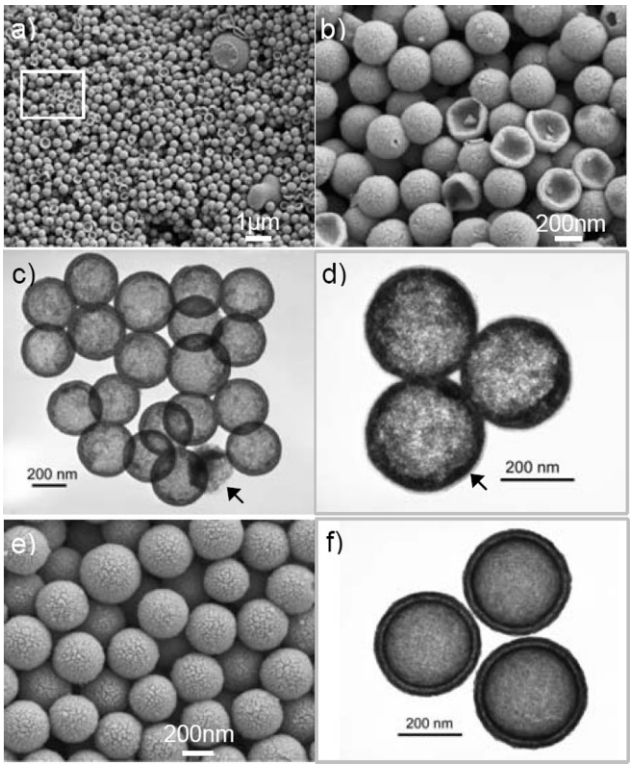

Figure 2. a,b) FESEM and c,d) TEM images of SnO_2@carbon hollow spheres. Arrows in c) and d) indicate carbon shells, b) corresponds to the area indicated by a white rectangle in a). e,f) Double-shelled SnO_2 hollow spheres.

double-shells do not collapse (Fig. 2e, f), but one can observe some broken hollow spheres (see Supporting Information). This observation suggests that such SnO_2@carbon coaxial shells should be quite elastic, which might prove advantageous for improving cycling performance. In addition, closer examination reveals that there are small holes on many SnO_2@carbon hollow spheres, created presumably during dissolution of the silica templates. Such ''nanoportals'' are also desirable for enhanced Li-ion diffusion, which enhances the charge rate capabilities. Because of its relatively low contrast, the outer carbon layer can be clearly seen from the TEM images (Fig. 2c and d), as indicated by arrows. Under optimized conditions, the GCP materials mainly deposit on SnO_2 shells. However, it should be pointed out that the formation of some carbon microspheres seems inevitable, as observed in Figure 2a. It is further observed from Figure 2d that the inner double-shell structure of SnO_2, unlike the bare SnO_2 hollow spheres (see Fig. 2f), does not appear well-defined any more due to shrinkage of the GCP shell during carbonization. It follows that the SnO_2 nanoparticles are closely attached onto the flexible carbon shell. Combining a hollow interior space and an elastic buffering shell, such a ''breathable'' nanoarchitecture is anticipated to offer great promise for improving cycle life of SnO_2-based anodes.

In general, a high-temperature process is required for carbon formation through chemical vapor deposition or carbonization of polymers. This renders it very challenging to prepare nanocomposite SnO_2–carbon anode materials with designed architecture, due to carbothermal reduction of SnO_2 forming low-melting point (232 °C) Sn. In this regard, hydrothermally derived GCP is advantageous because it can be carbonized at a temperature as low as 400 °C, while carbothermal reduction of SnO_2 takes place only when the temperature reaches about 600 °C.[28] As confirmed by X-ray diffraction (XRD) analysis (see Supporting Information), no elemental Sn is formed after carbonization at 500 °C, while the SnO_2 peaks are only slightly sharpened in comparison with SnO_2 double-shells. The carbon content in these SnO_2@carbon hollow nanospheres can be readily determined by thermogravimetric analysis (TGA) to be about 32.3 wt% (see Supporting Information).

We investigated the potential use of these SnO_2@carbon coaxial hollow nanospheres as an anode material for LIBs. Figure 3a shows the cyclic voltammograms (CV) for the first two cycles at a scan rate of 0.05 mV s^{-1} in the potential window of 3 V–5 mV. The CV behavior is generally consistent with the literature,[29] indicating the same electrochemical reaction pathway. Specifically, three reduction peaks are observed in the first cathodic scan. Two of them are around 1.64 and 0.98 V, which might be ascribed to the formation of solid electrolyte interface (SEI), and reduction of SnO_2 to Sn and Li_2O, respectively.[30,31] The third dominant peak between 0.6 and 0 V is known to arise from the formation of Li_xSn alloys. In agreement with this CV result, three poorly defined plateau regions can be identified in the first discharge voltage profile (see Supporting Information). The discharge–charge cycling performance is evaluated between 2 V and 5 mV at a 0.8 C (note that here C does not have the usual meaning but is defined as 625 mA g^{-1} in this work for easy denotation) rate up to 100 cycles, as shown in Figure 3b. As expected, these SnO_2@carbon coaxial hollow spheres manifest exceptional cyclability compared to other SnO_2-based anode materials.[8,13,29] Specifically, while the capacity decays gradually over the first 30 cycles, it stabilizes around 460 mA h g^{-1} for more than 100 cycles. After 100 cycles, the same cell was further evaluated for rate capability as shown in Figure 3c. When the current rate is first reduced from 0.8 to 0.32 C, a stable capacity of 520 mA h g^{-1} can be achieved. Afterward, the rate is increased stepwise up to 12 C. As an example, at a high rate of 4.8 C, the hollow spheres can still deliver a stable capacity of about 210 mA h g^{-1}. In other words, the discharge or charge process can be finished in about 4 min while still obtaining relatively high capacity. Remarkably, when the current rate is again reduced back to 0.32 C after more than 200 cycles, a stable high capacity of 500 mA h g^{-1} can be resumed. This result might suggest that the elastic hollow structure is indeed very ''breathable.''

It is well known that the cycling performance is highly dependent on the discharge/charge voltage window employed. In general, the cycling performance will be dramatically reduced with a wider discharge/charge voltage window because of the harsher conditions applied for the extraction of lithium. We also examined the cycling performance in the voltage window of 3 V–5 mV. Significantly, excellent cycling performance can still be obtained at a 0.8 C rate, producing a stable capacity of about 630 mA h g^{-1} after 80 cycles (see Supporting Information). Lastly, the cycling performance of these SnO_2@carbon coaxial hollow spheres is compared with that of SnO_2 hollow spheres under identical testing conditions (see Supporting Information). Because of the presence of about one-third by mass of barely

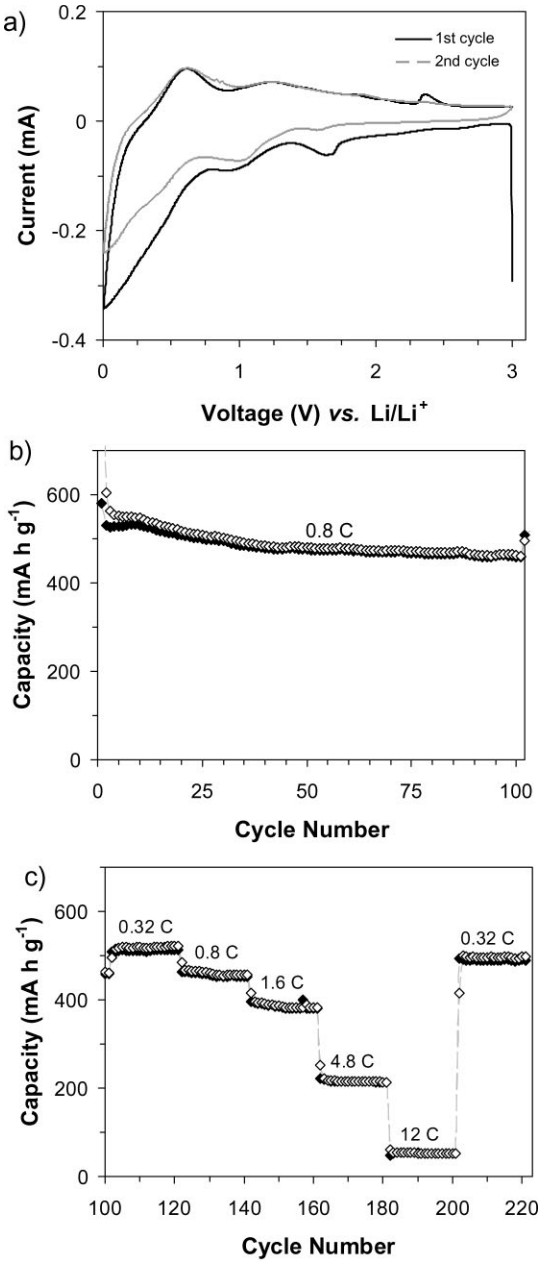

Figure 3. a) CV of SnO_2@carbon coaxial hollow spheres showing the first two cycles between 3 V and 5 mV at a scan rate of 0.05 mV s^{-1}. b) Capacities versus cycle number between 2 V and 5 mV at a 0.8 C rate ($C = 625$ mA g^{-1}). c) Cycling performance of the same cell at various rates after cycled for 100 cycles shown in b).

active amorphous carbon in the SnO_2@carbon, the initial capacity of SnO_2@carbon is about two-thirds of the capacity of bare SnO_2 sample. In agreement with the literature, the capacity of bare SnO_2 hollow spheres fades rapidly to about 69% of the initial value after only 20 cycles. After that, the capacity decays at a slower but almost constant rate to a value below that of SnO_2@carbon coaxial hollow spheres after about 46 cycles. It nevertheless should be noted that the capacity retention of these SnO_2 hollow spheres is significantly enhanced if compared to other SnO_2 nanostructures because of their large cavity space.[13,25,29] Still, our rationally designed SnO_2@carbon coaxial hollow spheres manifest superior cycling performance, namely, a stable capacity of about 500 mA h g^{-1} for at least 200 cycles.

In summary, we have rationally designed a functional nanoarchitecture, coaxial hollow spheres, for highly reversible lithium storage. We successfully demonstrated the concept by synthesizing coaxial SnO_2@carbon hollow spheres. This structure incorporates simultaneously two desirable design rationales for high-energy anode materials based on Li-metal alloying, hollow interior space, and carbon nanopainting. When evaluated for lithium-storage properties, these coaxial SnO_2@carbon hollow spheres indeed exhibit exceptional cycle life for at least several hundred cycles and rate capability. The superior performance may justify their potential use as high-performance anode materials for next-generation LIBs. The proof-of-concept structural design presented in this work should be valuable for the preparation of other electrode materials.

Experimental

Materials Synthesis: Monodisperse silica nanospheres (240–250 nm in diameter) were synthesized by the well-known Stöber's method [32]. Coating of SnO_2 double-shells on silica nanospheres was achieved using our previously reported protocol [27]. Afterward, glucose-derived carbon material was coated on SiO_2@SnO_2 by a simple hydrothermal process. In a typical synthesis, 0.3 g of as-prepared core/shell SiO_2@SnO_2 nanospheres was easily dispersed by ultrasonication in 20 mL of 0.5 M aqueous glucose solution. The suspension was transferred to a 40 mL Teflon-lined autoclave, which was then heated in an air-flow electric oven at 180 °C for 3 h. The product was harvested by centrifugation and washed with deionized water and ethanol at least five times. After drying at 50 °C, the resulting brown powder was carbonized at 500 °C for 4 h under inert atmosphere. Finally, SnO_2@carbon coaxial hollow spheres were obtained by dissolving the silica nanotemplates in a 2 M NaOH solution at 50 °C for 8 h.

Materials Characterization: Products were thoroughly characterized using XRD (Scintag PAD X, Cu Kα, $\lambda = 1.5406$ Å), FESEM (Hitachi S4500), and TEM (JEOL-1200EX, 120 kV, and FEI Tecnai T12, 120 kV). TGA was carried out under air flow of 60 mL min^{-1} using TA Instrument Q500 from room temperature to 550 °C with a heating rate of 3 °C min^{-1}.

Electrochemical Measurement: The electrochemical measurements were carried out using homemade Swagelok-type cells with lithium metal as the counter and reference electrodes at room temperature. The working electrode consisted of active material (SnO_2@carbon hollow spheres), conductivity agent (carbon black, Super-P-Li), and polymer binder (polyvinylidene difluoride, PVDF, Aldrich) in a weight ratio of around 80:10:10. The active material loading in each electrode disc (about 12 mm in diameter) was typically 1–2 mg, corresponding to about 1.5 mg cm^{-2}. The electrolyte was 1 M $LiPF_6$ in a 50:50 w/w mixture of ethylene carbonate and diethyl carbonate. Cell assembly was carried out in an Ar-filled glove box with the concentrations of moisture and oxygen below 1 ppm. Charge–discharge cycles of the cells were measured in a fixed voltage window (see main text) at a constant current density using a Maccor 4304 battery tester. Both the *C* rate and specific capacity are corrected based on the mass of SnO_2@carbon coaxial hollow spheres, while excluding possible impurities such as remnant silica and base from elemental analysis. 1C is defined as 625 mA g^{-1} for easy denotation.

Acknowledgements

This publication was based on work supported by Award No. KUS-C1-018-02, made by King Abdullah University of Science and Technology (KAUST). We are also grateful to the National Science Foundation (DMR 0404278) for partial support. Facilities available through the Cornell Center for

Materials Research (CCMR), and Cornell Integrated Microscopy Center (CIMC) were used for this study. Supporting Information is available online from Wiley InterScience or from the author. This article has been amended for print publication.

Received: November 22, 2008
Revised: February 7, 2009
Published online: March 25, 2009

[1] J. M. Tarascon, M. Armand, *Nature* **2001**, *414*, 359.
[2] Y. Idota, T. Kubota, A. Matsufuji, Y. Maekawa, T. Miyasaka, *Science* **1997**, *276*, 1395.
[3] J. Hassoun, S. Panero, P. Simon, P. L. Taberna, B. Scrosati, *Adv. Mater.* **2007**, *19*, 1632.
[4] K. T. Nam, D. W. Kim, P. J. Yoo, C. Y. Chiang, N. Meethong, P. T. Hammond, Y. M. Chiang, A. M. Belcher, *Science* **2006**, *312*, 885.
[5] L. Taberna, S. Mitra, P. Poizot, P. Simon, J. M. Tarascon, *Nat. Mater.* **2006**, *5*, 567.
[6] K. Kang, Y. S. Meng, J. Breger, C. P. Grey, G. Ceder, *Science* **2006**, *311*, 977.
[7] G. Derrien, J. Hassoun, S. Panero, B. Scrosati, *Adv. Mater.* **2007**, *19*, 2336.
[8] M. S. Park, G. X. Wang, Y. M. Kang, D. Wexler, S. X. Dou, H. K. Liu, *Angew. Chem. Int. Ed.* **2007**, *46*, 750.
[9] M. Noh, Y. Kwon, H. Lee, J. Cho, Y. Kim, M. G. Kim, *Chem. Mater.* **2005**, *17*, 1926.
[10] D. Larcher, S. Beattie, M. Morcrette, K. Edstroem, J. C. Jumas, J. M. Tarascon, *J. Mater. Chem.* **2007**, *17*, 3759.
[11] Y. G. Guo, Y. S. Hu, W. Sigle, J. Maier, *Adv. Mater.* **2007**, *19*, 2087.
[12] X. W. Lou, L. A. Archer, Z. C. Yang, *Adv. Mater.* **2008**, *20*, 3987.
[13] X. W. Lou, Y. Wang, C. Yuan, J. Y. Lee, L. A. Archer, *Adv. Mater.* **2006**, *18*, 2325.
[14] Y. Wang, H. C. Zeng, J. Y. Lee, *Adv. Mater.* **2006**, *18*, 645.
[15] X. W. Lou, D. Deng, J. Y. Lee, J. Feng, L. A. Archer, *Adv. Mater.* **2008**, *20*, 258.
[16] H. Ma, F. Y. Cheng, J. Chen, J. Z. Zhao, C. S. Li, Z. L. Tao, J. Liang, *Adv. Mater.* **2007**, *19*, 4067.
[17] S. J. Han, B. C. Jang, T. Kim, S. M. Oh, T. Hyeon, *Adv. Funct. Mater.* **2005**, *15*, 1845.
[18] X. W. Lou, L. A. Archer, *Adv. Mater.* **2008**, *20*, 1853.
[19] K. T. Lee, Y. S. Jung, S. M. Oh, *J. Am. Chem. Soc.* **2003**, *125*, 5652.
[20] W. M. Zhang, J. S. Hu, Y. G. Guo, S. F. Zheng, L. S. Zhong, W. G. Song, L. J. Wan, *Adv. Mater.* **2008**, *20*, 1160.
[21] Z. H. Wen, Q. Wang, Q. Zhang, J. H. Li, *Adv. Funct. Mater.* **2007**, *17*, 2772.
[22] S. H. Ng, J. Z. Wang, D. Wexler, K. Konstantinov, Z. P. Guo, H. K. Liu, *Angew. Chem. Int. Ed.* **2006**, *45*, 6896.
[23] M. S. Park, S. A. Needham, G. X. Wang, Y. M. Kang, J. S. Park, S. X. Dou, H. K. Liu, *Chem. Mater.* **2007**, *19*, 2406.
[24] Q. Fan, P. J. Chupas, M. S. Whittingham, *Electrochem. Solid State Lett.* **2007**, *10*, A274.
[25] X. W. Lou, J. S. Chen, L. A. Archer, **2008**, submitted.
[26] X. W. Lou, D. Deng, J. Y. Lee, L. A. Archer, *Chem. Mater.* **2008**, *20*, 6562.
[27] X. W. Lou, C. Yuan, L. A. Archer, *Small* **2007**, *3*, 261.
[28] X. M. Sun, J. F. Liu, Y. D. Li, *Chem. Mater.* **2006**, *18*, 3486.
[29] M. S. Park, Y. M. Kang, G. X. Wang, S. X. Doti, H. K. Liu, *Adv. Funct. Mater.* **2008**, *18*, 455.
[30] R. Demir-Cakan, Y. S. Hu, M. Antonietti, J. Maier, M. M. Titirici, *Chem. Mater.* **2008**, *20*, 1227.
[31] J. C. Lytle, H. W. Yan, N. S. Ergang, W. H. Smyrl, A. Stein, *J. Mater. Chem.* **2004**, *14*, 1616.
[32] W. Stober, A. Fink, E. Bohn, *J. Colloid Interface Sci.* **1968**, *26*, 62.